Trends in Extreme Rainfall Frequency in the Contiguous United States: Attribution to Climate Change and Climate Variability Modes

SAMAN ARMAL, NARESH DEVINENI, AND REZA KHANBILVARDI

Department of Civil Engineering, NOAA Center for Earth System Sciences and Remote Sensing Technologies, Center for Water Resources and Environmental Research, City College, City University of New York, New York, New York

(Manuscript received 19 February 2017, in final form 24 August 2017)

ABSTRACT

This study presents a systematic analysis for identifying and attributing trends in the annual frequency of extreme rainfall events across the contiguous United States to climate change and climate variability modes. A Bayesian multilevel model is developed for 1244 rainfall stations simultaneously to test the null hypothesis of no trend and verify two alternate hypotheses: trend can be attributed to changes in global surface temperature anomalies or to a combination of well-known cyclical climate modes with varying quasiperiodicities and global surface temperature anomalies. The Bayesian multilevel model provides the opportunity to pool information across stations and reduce the parameter estimation uncertainty, hence identifying the trends better. The choice of the best alternate hypothesis is made based on the Watanabe–Akaike information criterion, a Bayesian pointwise predictive accuracy measure. Statistically significant time trends are observed in 742 of the 1244 stations. Trends in 409 of these stations can be attributed to changes in global surface temperature anomalies. These stations are predominantly found in the U.S. Southeast and Northeast climate regions. The trends in 274 of these stations can be attributed to El Niño–Southern Oscillation, the North Atlantic Oscillation, the Pacific decadal oscillation, and the Atlantic multidecadal oscillation along with changes in global surface temperature anomalies. These stations are mainly found in the U.S. Northwest, West, and Southwest climate regions.

1. Introduction

There is a large body of literature that supports the contribution of humans to global warming (e.g., Ring et al. 2012; IPCC 2013). The rise of temperature and the resulting increase in the atmosphere's water-holding capacity intensify the global water cycle (Huntington 2006; Trenberth 2011) and lead to more severe and frequent precipitation events (Alfieri et al. 2015; Min et al. 2011). This is particularly felt in the high latitudes and tropical regions, and during the winter seasons of the northern midlatitudes (Seneviratne et al. 2012). During the recent years, efforts have been made to investigate the trends in extreme precipitation and their association with climate change at the global (e.g., Westra et al. 2013; Alexander et al. 2006; Asadieh and Krakauer 2015; Fischer and Knutti 2014), national (Balling and Goodrich 2011; Karl and Knight 1998; Groisman et al. 2004; Sun and Lall 2015; Zhu 2013), and regional scales (Villarini et al. 2011; Parr et al. 2015).

However, anthropogenic forcing cannot solely explain the trend in climate observations, and the actual trajectory is highly dependent on internal variability of the natural climate (Seneviratne et al. 2012). Since climate has a cyclical nature, in a particular region, its manifestation can be entirely different for a given decade or century. Many studies have documented the effect of natural climate variability on rainfall patterns including the impact of El Niño–Southern Oscillation (ENSO), the interdecadal Pacific oscillation (IPO), the Pacific decadal oscillation (PDO), the North Atlantic Oscillation (NAO), and the Atlantic multidecadal oscillation (AMO) on precipitation extremes and rainfall regime in the United States (Gershunov and Cayan 2003), South America (Haylock et al. 2006), eastern Africa (Schreck and Semazzi 2004), India (Zhang and Delworth 2006), Australia (Verdon et al. 2004; Samuel and Sivapalan 2008; Kamruzzaman et al. 2013; Cai and Van Rensch 2012; Sun et al. 2014; Westra et al. 2015), Europe (Willems 2013; Cioffi et al.

Corresponding author: Saman Armal, sarmal000@citymail.cuny.edu

DOI: 10.1175/JCLI-D-17-0106.1

2015), and the Southern Hemisphere (Gergis and Henley 2017). Hence, it is important to tease out the influence of anthropogenic forcing and natural climate variability on the occurrence of extreme events in an integrated framework, an objective that has motivated this study. This paper provides a hypothesis-driven methodology to understand the association of trends in extreme rainfall event frequency to anthropogenic forcing and natural climate variability over the contiguous United States.

A standard method that has been adopted in the past is to perform a parametric/nonparametric trend analysis, or to fit a distribution based on well-known probability models on a limited time series data of block maxima or peaks over a threshold. For instance, Asadieh and Krakauer (2015) have used linear regression and Mann–Kendall trend tests on annual maximum daily rainfall to quantify the global trends in the last century. Westra et al. (2013) have used a nonstationary generalized extreme value distribution (GEV) for annual maximum rainfall data where the location parameter is informed by global near-surface temperature to quantify the association between the precipitation extremes and changing temperatures. Similarly, Sun and Lall (2015) have used a nonstationary hierarchical Bayesian GEV cluster model on annual maximum rainfall data over the United States and quantified spatially coherent time trends. Scian and Pierini (2013) have adopted a gamma distribution model to identify the seasonal trends in the wet and dry extremes. Villarini et al. (2011) have used various extreme value distribution models, changepoint analysis and Mann–Kendall trend tests to quantify changes in extreme rainfall in the U.S. Midwest.

The methods described above typically restrict the objective to examining whether there is a positive or negative trend in the extreme events, or whether there are changes in the parameters before and after a certain time (e.g., pre-1960 vs post-1960). However, as mentioned above, the quasiperiodic nature of climate leads to periodic runs of wet or dry years regionally. These cyclical variabilities often translate into periods of increasing or decreasing extreme events depending on the phase of the climate. Hence, based on the length of the records available at a particular station, the trend can be overestimated or can lead to a false signal if one does not account for the full climate information. This investigation follows a systematic hypothesis-based learning approach that attributes the time trends in extreme events to anthropogenic forcings (using global near-surface temperature as a proxy) and well-known natural processes such as the interannual (using ENSO index as a proxy) to decadal (using the NAO and PDO indices as proxies) to multidecadal (using the AMO index as a proxy) oscillations driven by ocean–atmosphere interactions.

Given that there are a large number of rainfall stations across the contiguous United States that may exhibit similar behavior regionally, we employed a Bayesian multilevel modeling approach to group information and to reduce parameter estimation uncertainty. A systematic learning structure shapes the study to identify the spatial controls of anthropogenic forcing and various modes of natural variability, through the inclusion of global near-surface temperature and climate variables into the inference of the Bayesian model. We assume a Poisson process model for the number of days with rainfall greater than a threshold (95th percentile of the rainfall data for the whole period of record). This assumption is tested using a Kolmogorov–Smirnov (KS) test. In our analysis we consider two hypotheses: 1) the monotonic trend in the annual frequency of extreme rainfall events is solely attributed to anthropogenic forcing, and 2) the monotonic trend in the annual frequency of extreme rainfall events is attributed to anthropogenic forcing and cyclical climate variability. The models get information from global near-surface temperature and climate indices, and the residual trends for each hypothesis are examined.

As a motivation for our study, in the next section, a simple simulation experiment is presented to explicate the role of climate and the length of the available time series in detecting the trends. Section 3 presents the rainfall station data for the contiguous United States, its filtering procedure, the data used for global near-surface temperature, and the climate indices. In section 4, we introduce the Bayesian multilevel models for trend identification in a systematic hypothesis framework. In section 5, we present the trend results and their regional variability under each hypothesis. Finally, in section 6, we present a discussion and summary of the study.

2. The role of climate in detecting trends: A simulation experiment

A simulation-based experiment is designed to illustrate the importance of accounting for periodic climate oscillations in trend analysis of hydroclimatic variables. We argue that a simple time trend analysis conducted to capture increases or decreases in hydroclimatic variables can often show false positives depending on the length of the record (time series) used and/or depending on the phase of the climate signal. For example, let us suppose that rainfall in a given region is influenced by interannual (e.g., ENSO), decadal (e.g., PDO), and multidecadal (e.g., AMO) climate oscillations. Under this premise, any given decade or a block of time can manifest as runs of wet or dry years. If the region has observed records long enough to capture these cyclicities, periods of wet years will be transposed by periods of dry years and the

resulting long-term time trend in rainfall will be nonexistent. On the contrary, if the region has limited observed records, one can detect a long-term increasing or decreasing trend in the data depending on whether the climate is manifested as wet or dry years. To demonstrate this further, we create the following experimental setup.

Consider that the annual frequency of extreme rainfall events (i.e., the number of rainfall events exceeding a threshold per year) follows a Poisson process with a rate parameter that depends on several periodic modes (cyclical trends):

$$Y_t \sim \text{Poisson}(\lambda_t) \quad \text{and} \tag{1}$$

$$\lambda_t = \alpha + \beta_1 \sin(\omega_1 t) + \beta_2 \sin(\omega_2 t) + \beta_3 \sin(\omega_3 t) + \beta_4 \sin(\omega_4 t). \tag{2}$$

Note that this is a stationary process (i.e., there is no long-term time trend in the model).

The following parameter values are assumed: an average of 10 events per year (i.e., $\alpha = 10$), a unit amplitude for all the periodic waves (i.e., β_1, β_2, β_3, and $\beta_4 = 1$), and four distinct frequencies (ω_1, ω_2, ω_3, and ω_4) that replicate interannual (periodicity of 5 yr), decadal (periodicity of 10 yr), bidecadal (periodicity of 20 yr), and century (periodicity of 100 yr) scales of climate variability. Next, we perform the following steps:

1) The Poisson process model is used to generate 10 000 years as the population.
2) A contiguous block of m years (m varies from 10 to 1000 yr) from the rainfall extremes data Y and the predictor data (four periodic cycles) are considered as a sample from the population.
3) For each m, 1000 random blocks of m years are drawn from the 10 000-yr population data, a generalized linear time trend model M_1 is fit to each random block, and the trend coefficient is verified for statistical significance at the 1% significance level. Notice that M_1 does not use the periodic cycles as predictors; hence, for any random block of m years, there is a chance of observing a monotonic time trend. We record these as false positives (since the population data arise from a stationary process) and compute the overall percentage false positives out of the 1000 random blocks.
4) For the same m-yr random block of data, the generalized linear model M_2 is now fit to the rainfall extremes data and the time block and the periodic cycles. We record the false positives after accounting for the full cyclical trends. Based on our hypothesis, the random blocks that exhibited statistically significant monotonic time trends before accounting for the cyclical patterns should now not show this trend once the predictors are included.

Figure 1 presents the results of this experiment. The population data (i.e., the 10 000 years of rainfall extremes annual frequency data generated from the Poisson process model) are shown in Fig. 1a. A randomly selected segment of 80 yr is shown in Fig. 1b. Notice that this sample shows an apparent monotonic increasing time trend. This is referred to as a false positive. A generalized linear model fit to the sample data against time ($y_t = a_0 + b_0 T + \varepsilon_t$) shows that the slope is positive with a p value of 0.00195 (a statistical significance beyond the 99% confidence level). As an alternative, we fit another generalized linear model to the same sample data, but with time, and the four cyclical predictors [$\sin(\omega_1 t)$, $\sin(\omega_2 t)$, $\sin(\omega_3 t)$, and $\sin(\omega_4 t)$] coming from the same segment [$y_t = a_0 + b_0 T + b_1 \sin(\omega_1 t) + b_2 \sin(\omega_2 t) + b_3 \sin(\omega_3 t) + b_4 \sin(\omega_4 t) + \varepsilon_t$]. All the coefficients are positive with respective p values of 0.1526, 0.0740, 0.0544, 0.0417, and 0.5780. It is observed that the significance of the time trend coefficient is nullified with the inclusion of the cyclical predictors. In this segment of the data, the monotonic increase in rainfall extremes can be explained by a combination of 10- and 20-yr periodic cycles.

Figure 1c presents the comparison of percentage false positives from M_1 (only time as the predictor) and M_2 (time and climate signals as predictors) for various sizes of the random segments. We vary the segment size from 10 to 1000 at increments of 10, for a total of 100 segments. In Fig. 1c, the color of the dot indicates the size of the segment. It ranges from dark blue for very small segment sizes to dark red for very large segment sizes. One can analogously compare this to having stations with very small sample sizes to stations with very large sample sizes. We estimate the false positives as the number of random models out of 1000 that show a time trend coefficient that is significant at the 1% confidence level. From Fig. 1, we observe that the percentage of false positives for M_1 range from 0 for large sample sizes to around 15 for small sample sizes. However, the percentage of false positives for M_2 only range from 0 (large sample sizes) to 1 (small sample sizes), which is expected under random chance at a 1% significance level. In Fig. 1, two important observations can be made: 1) a large sample size is needed to identify the monotonic time trends robustly, and 2) accounting for the cyclical patterns (climate signals) will help reduce the false positives regardless of the sample size. While long records of hydroclimatic variables will help better estimate the parameter uncertainty, we propose a climate-informed trend analysis model that can decompose the underlying climate signals while attributing the trends in the residual noise to factors outside the internal variability.

With this synthetic experiment as motivation, we proceed with the systematic hypothesis-driven approach

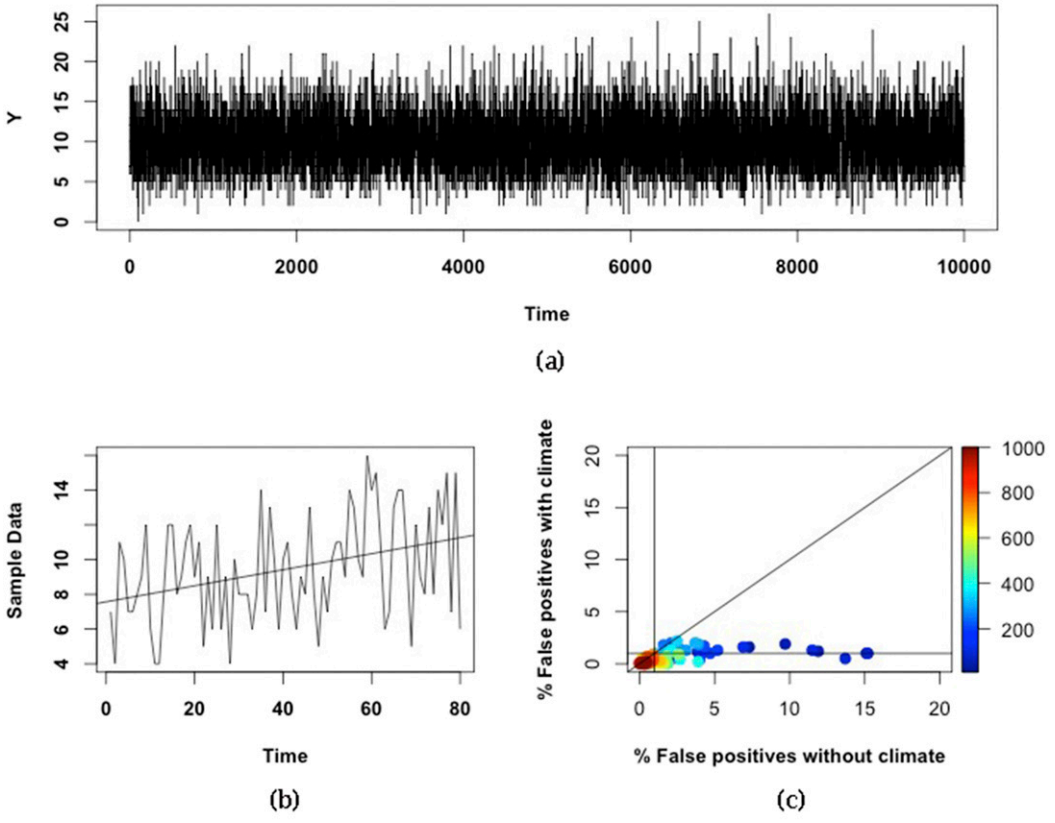

FIG. 1. (a) The population data generated from the Poisson process model. (b) A randomly selected segment of 80 yr. This sample shows an apparent monotonic increasing time trend. (c) The comparison of percentage false positives between M_1 and M_2 for various sizes of the random segments. We vary the segment size from 10 to 1000 at increments of 10, for a total of 100 segments. The color of the dot indicates the size of the segment. It ranges from dark blue for very small segment sizes to dark red for very large segment sizes. We estimate the false positives as the number of random models out of 1000 that show a time trend coefficient that is significant at the 1% confidence level. It is observed that the percentage false positives for M_1 range from 0 for large sample sizes to around 15 for small sample sizes. However, the percentage false positives for M_2 only range from 0 (large sample sizes) to 1 (small sample sizes), which is expected under random chance at a 1% significance level.

for trend identification in rainfall extreme frequency across the contiguous United States. Unlike the experimental setup presented in this section, we make no assumptions as to the stationarity of the process, and try to learn it in a systematic way by first attributing monotonic time trend to only anthropogenic influences (global near-surface temperature) and then examining for well-known large-scale climate indicators.

3. Data and processing

a. *Rainfall data*

Using data from the Global Historical Climatology Network (GHCN; https://www.ncdc.noaa.gov/data-access/land-based-station-data/land-based-datasets/global-historical-climatology-network-ghcn), we collected 12 244 stations across the United States and extracted the total daily precipitation from those that have data from 1900 to 2014 (115 years). From these data, we selected high-quality stations using the following procedure for each station: First, any year with more than 72 days (20%) of missing data are flagged as a missing year. Next, only stations that have at least 92 years of complete data (i.e., less than 20% missing) are selected. This process yielded 1244 stations across the contiguous United States. Figure 2a shows the spatial distribution of these stations along with the number of years of available data for each station. Figure 2b shows the boundaries of the nine climate regions (Karl and Koss 1984).

b. *Global near-surface temperature*

Globally averaged near-surface temperature serves as a proxy for anthropogenic forcing that can increase the rainfall extremes. For this study, we used the annual

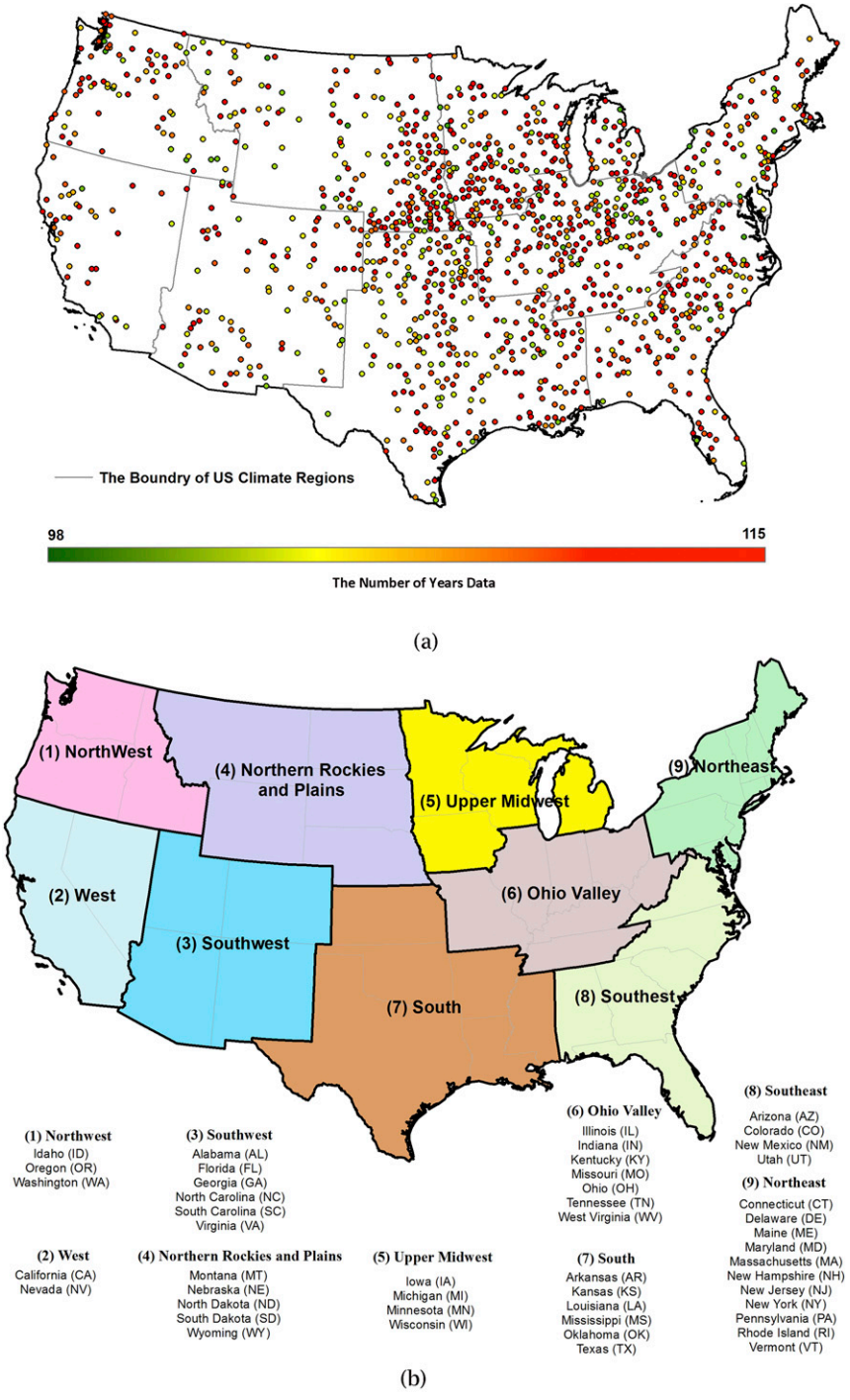

FIG. 2. (a) The location of selected stations used in the model. (b) The nine climate regions over the contiguous United States (adapted from https://www.ncdc.noaa.gov/monitoring-references/maps/us-climate-regions.php).

near-surface global temperature anomalies (with respect to 1951–80) available from the National Aeronautics and Space Administration (NASA) Goddard Institute for Space Studies (GISS) (Hansen et al. 2010). Westra et al. (2013) have used this data as the covariate in their non-stationary trend model for annual maximum precipitation globally. Recently, Sutton et al. (2015) have shown that globally averaged near-surface temperature

(GST) can be related to local climate and can provide a means to guide climate change attribution studies.

c. ENSO

Several studies (e.g., Gershunov and Cayan 2003; Cayan et al. 1999) have confirmed the noticeable impact of ENSO on extreme precipitation patterns in the United States. The El Niño warm phase is associated with intense precipitation in the U.S. Southeast (Eichler and Higgins 2006) and shift of anomalously intense precipitation from the U.S. Southwest toward the U.S North region (Meehl et al. 2007). Similarly, the La Niña cold phase is found to yield a positive anomaly in the Southwest (Gershunov and Cayan 2003; Castello and Shelton 2004). The Niño-3.4 index was obtained from the Royal Netherlands Meteorological Institute's (KNMI) Climate Explorer (http://climexp.knmi.nl) and aggregated from monthly to the average yearly data.

d. AMO

The findings of Enfield et al. (2001) explain that the warming phase of the AMO is likely to be associated with a decrease in annual rainfall totals over the United States. Other studies suggested that the warm phase of the AMO is one driving factor in the increase of rainfall intensity (Curtis 2008) and duration (Teegavarapu et al. 2013) in central and southern Florida. The AMO index used in the model has been calculated as the average of the monthly Hadley Centre Sea Ice and Sea Surface Temperature dataset (HadISST) of sea surface temperature anomalies (van Oldenborgh et al. 2009).

e. NAO

The NAO is associated with increases in precipitation frequency and positive daily rainfall anomalies in the northern United States and decreases in the southern United States (Durkee et al. 2008). Archambault et al. (2008) have also reported that during the active phase, the NAO favors the moisture transport and relatively wet conditions near the eastern coast of the United States.

f. PDO

The PDO in the warm phase can amplify the modulating effect of El Niño, and alternate with the La Niña teleconnection with regard to winter precipitation in the western United States (Gershunov 1998; McCabe and Dettinger 1999). Additionally, in the years of neutral ENSO and cold PDO, more than 80% of western U.S. climate divisions are drier than that of any other ENSO and PDO combination (Goodrich 2007). The fact that the long-term effect of PDO can extend up to three decades (Mantua and Hare 2002) emphasizes its importance.

The PDO (https://www.ncdc.noaa.gov/teleconnections/pdo/) and NAO (https://climatedataguide.ucar.edu/climate-data/hurrell-north-atlantic-oscillation-nao-index-station-based) indices are obtained from NOAA's Extended Reconstructed Sea Surface Temperature and the station-based difference of normalized sea level pressure, respectively.

4. Methodology

Unlike several prior investigations of trends in hydroclimatic variables that verify the hypothesis of no trend using standard parametric or nonparametric tests, here we introduce a framework where systematic hypotheses are tested and compared using a set of models. The hypotheses are postulated to attribute the trends (if identified) to appropriate natural or anthropogenic forcings. We start with testing the null hypothesis that there is no trend, and the time series is a random draw from a probability distribution with parameters invariant to time. If the null hypothesis of no trend is rejected, we explore two alternate hypotheses to explain the trends. In the first alternate hypothesis, our proposition is that the detected time trend is solely due to anthropogenic forcings. In our case, we assume GST as a proxy for anthropogenic forcings. In the second alternate hypothesis, we postulate that the detected time trend is due to anthropogenic forcings or due to cyclical climate influences, or some combination thereof. The corresponding residual time-trend analysis for the two hypotheses explains whether the long-term natural variability or changing climate dominates the frequency of extreme rainfall events.

a. Choice of rainfall extremes and modeling framework

We consider the total number of days each year with rainfall events exceeding a threshold P^* as the measure of extremes. The 95th percentile of the daily nonzero rainfall series is considered as the threshold P^* for each station. The time series of the frequency of extreme rainfall at each station is thus given as

$$Y_{it} = \sum_{j=1}^{\mathrm{Nd}} \delta_{it}^{j} \quad \text{and} \tag{3}$$

$$\delta_{it}^{j} = \begin{cases} 1, & \text{if} \quad P_{it}^{j} \geq P_{i}^{*} \\ 0, & \text{if} \quad P_{it}^{j} < P_{i}^{*} \end{cases}, \tag{4}$$

where t is the year (1900–2014), i is the station index, P_{it}^{j} is the daily rainfall for the jth day for year t at station i, and P_i^* is the rainfall exceedance threshold for station i. Also, Nd is the number of days in the year (365 or 366

for leap years), and δ is the binary indicator function. A series of Bayesian multilevel generalized linear models (Gelman et al. 2003; Gelman and Hill 2006) with different possible explanations of the underlying trends in Y_{it} are presented next. A key aspect of the multilevel–hierarchical models is that the observed data Y_{it} can be modeled conditionally on certain parameters linked to time-varying exogenous variables, while the parameters themselves can be modeled conditionally on certain hyperparameters linked to regionally varying predictors to capture at-station and across-station variability simultaneously. Multilevel models also facilitate the pooling of information from multiple similarly behaving stations, thereby reducing the uncertainty in estimating the coefficients and improving the model reliability. They also allow us to study the relationships of the parameters to station level predictors.

Our goal is to estimate the trend in the frequency of rainfall extremes for each of the 1244 identified stations in the contiguous United States. The time series (1900–2014) of the rainfall extreme event frequency in each station is informed by time, anthropogenic, and climate covariates (depending on the particular hypothesis). Besides, we have climatological attributes (measure of average climatic conditions and elevation) as station level predictors. The basic idea is that a particular covariate may inform the time series at each of the stations. If the influences were the same, pooling all the data into the same regression would be effective since that would reduce the uncertainty associated with parameter estimation. However, the influence of the covariates across the stations may vary systematically due to local conditions. The multilevel model can be used for structuring this information (within and across stations) by considering multiple levels of modeling. The individual trend coefficients for each station on each covariate are estimated at the first level. The errors at the first level represent the within station variations that can be attributed to reporting errors and residual variability beyond what is explained by the covariates. The second level informs these trend coefficients across stations using local climatological features such as elevation and mean annual precipitation and its variability. The errors at the second level represent variations in the trends between the stations that cannot be explained by station level climatological predictors.

Bayesian multilevel–hierarchical models that combine data sources or model extreme events vary widely in approach. Cooley et al. (2007) estimated the magnitude and return frequency of extreme daily rainfall by fitting Bayesian hierarchical models to Colorado gauge measurements assuming a generalized Pareto distribution. Coles and Tawn (1996) developed Bayesian techniques to analyze daily rainfall series. Sang and Gelfand (2010) proposed a hierarchical Bayesian modeling approach for spatial rainfall extremes. Schliep et al. (2010) developed hierarchical spatial models for analyzing rainfall extremes from various regional climate models. Readers are referred to Renard et al. (2013) for a detailed review of Bayesian methods for nonstationary extreme value analysis.

b. *Null hypothesis H_0: There is no monotonic trend in the annual frequency of extreme rainfall events*

We begin our investigation with the null hypothesis that there is no monotonic trend in the annual frequency of extreme rainfall events. We test this hypothesis using a Bayesian multilevel generalized linear model. The frequency of rainfall extremes $\mathbf{Y}$ is assumed to come from a distribution (process model) with a probability density function $f(\mathbf{Y} \mid \boldsymbol{\theta})$, where $\boldsymbol{\theta}$ is the parameter vector. In the current application, since we are estimating the number of days (counts) in an interval, we consider that $\mathbf{Y}$ follows a Poisson distribution. The first level of the model considers that in each station i, Y_{it} is described by a Poisson distribution with time-varying rate parameter λ_{it} that is informed by a regression on time t with intercepts α_0^i and a 1×1244 regression coefficient matrix $\boldsymbol{\beta}_0$. The second level of the model considers that the intercepts $\boldsymbol{\alpha}_0$ and the regression coefficient matrix $\boldsymbol{\beta}_0$ can be estimated using the station level location and climatological predictors. The multilevel structure allows parameterizing the time trend across stations that may have a disparate range or scale of values:

$$Y_{it} \sim \text{Poisson}(\lambda_{it}), \tag{5}$$

$$\ln(\lambda_{it}) = \alpha_0^i + \beta_0^i t, \tag{6}$$

$$\alpha_0^i \sim N(a_{00} + a_{01}\overline{P}_i + a_{02}\text{CV}_i + a_{03}E_i, \sigma_{\alpha_0}^2), \quad \text{and} \tag{7}$$

$$\beta_0^i \sim N(b_{00} + b_{01}\overline{P}_i + b_{02}\text{CV}_i + b_{03}E_i, \sigma_{\beta_0}^2), \tag{8}$$

where Y_{it} is the number of extreme rainfall days in year t at station i, t is the indicator of time (1900–2014), and $\overline{P}_i$, CV_i, and E_i are the average annual rainfall, coefficient of variation of annual rainfall, and elevation of station i. Since the effect of the trend (response) parameters depends on the region, the second level helps retain the regional characteristics and convey the variation into the posterior simulation. Renard (2011) also proposed the station-specific covariates in the second level as a means to retain the spatial dependency in the model. The errors with variance $\sigma_{\alpha_0}^2$ and $\sigma_{\beta_0}^2$ represent variation in the intercept and trend between stations beyond what is explained by the station

level elevation and climatological predictors. For each station i, we investigate whether the trend coefficient β_0^i is significantly different from zero or not. We compute the probability that the posterior distribution of β_0^i is greater than zero (p value) and evaluate its statistical significance at 1% level of significance (i.e., the probability of incorrectly rejecting the null hypothesis). If the null hypothesis that there is no monotonic time trend in the annual frequency of rainfall extremes is rejected, we postulate the following alternate hypotheses to explain the monotonic time trend.

c. Alternate hypothesis H_1: The monotonic trend in the annual frequency of extreme rainfall events is solely attributed to anthropogenic forcing

An increasing atmospheric temperature can lead to an increase in the atmospheric water-holding capacity (as governed by the Clausius–Clapeyron equation), which in turn can cause increasing extreme precipitation (Trenberth et al. 2003). Two climate model experiments (the Hadley Centre's high-resolution climate prediction model UKHI and Australia's CSIRO9 model; Hennessy et al. 1997) indicated that precipitation has been shifting toward more intense convective events and fewer moderate nonconvective events in the mid-to-low latitudes, and toward more moderate and heavy events in the high latitudes. In the first alternate hypothesis, we propose that the monotonic trend in the annual frequency of rainfall extremes is solely due to anthropogenic forcing; hence, Y_{it} should vary in response to GST variability. Westra et al. (2013) have also used GST data to investigate the trends in annual maximum rainfall events globally.

$$Y_{it} \sim \text{Poisson}(\lambda_{it}), \tag{9}$$

$$\ln(\lambda_{it}) = \alpha_1^i + \beta_1^i \text{GST}_t, \tag{10}$$

$$\alpha_1^i \sim N(a_{10} + a_{11}\overline{P}_i + a_{12}\text{CV}_i + a_{13}E_i, \sigma_{\alpha_1}^2), \quad \text{and} \tag{11}$$

$$\beta_1^i \sim N(b_{10} + b_{11}\overline{P}_i + b_{12}\text{CV}_i + b_{13}E_i, \sigma_{\beta_1}^2), \tag{12}$$

where the GST is from 1900 to 2014, the exogenous predictor.

d. Alternate hypothesis H_2: The monotonic trend in the annual frequency of extreme rainfall events is attributed to anthropogenic forcing and cyclical climate variability

Next, we propose a second alternate hypothesis H_2, that the monotonic time trend can be attributed to cyclical climate variability and anthropogenic forcing. The persistence in the climate system can often manifest as periods of wet or dry years, which in turn can translate into periods of increasing or decreasing extreme events. Using climate indicators as predictors in addition to GST will help contrast these influences. We use four climate predictors with different quasiperiodic cycles ranging from interannual to decadal and to multidecadal scales. The rate parameter λ_{it} of the data distribution is informed by GST, ENSO, NAO, PDO, and AMO. At the second level, the trend coefficients are informed by the station predictors. A multivariate normal distribution is used to model the joint behavior of the climate trend coefficients:

$$Y_{it} \sim \text{Poisson}(\lambda_{it}), \tag{13}$$

$$\ln(\lambda_{it}) = \alpha_2^i + \beta_2^i \text{GST}_t + \beta_{\text{enso}}^i \text{ENSO}_t + \beta_{\text{nao}}^i \text{NAO}_t + \beta_{\text{pdo}}^i \text{PDO}_t + \beta_{\text{amo}}^i \text{AMO}_t, \tag{14}$$

$$\alpha_2^i \sim N(a_{20} + a_{21}\overline{P}_i + a_{22}\text{CV}_i + a_{23}E_i, \sigma_{\alpha_2}^2), \tag{15}$$

$$\beta_2^i \sim N(b_{20} + b_{21}\overline{P}_i + b_{22}\text{CV}_i + b_{23}E_i, \sigma_{\beta_2}^2), \quad \text{and} \tag{16}$$

$$\begin{pmatrix} \beta_{\text{enso}}^i \\ \beta_{\text{nao}}^i \\ \beta_{\text{pdo}}^i \\ \beta_{\text{amo}}^i \end{pmatrix} \sim N\left[\begin{pmatrix} a_0^{\text{enso}} + a_1^{\text{enso}}\overline{P}_i + a_2^{\text{enso}}\text{CV}_i + a_3^{\text{enso}}E_i \\ a_0^{\text{nao}} + a_1^{\text{nao}}\overline{P}_i + a_2^{\text{nao}}\text{CV}_i + a_3^{\text{nao}}E_i \\ a_0^{\text{pdo}} + a_1^{\text{pdo}}\overline{P}_i + a_2^{\text{pdo}}\text{CV}_i + a_3^{\text{pdo}}E_i \\ a_0^{\text{amo}} + a_1^{\text{amo}}\overline{P}_i + a_2^{\text{amo}}\text{CV}_i + a_3^{\text{amo}}E_i \end{pmatrix}, \Sigma \right], \tag{17}$$

where GST is as before, and ENSO and the NAO, PDO, and AMO are the exogenous climate indicators. Similar to H_0 and H_1, in this model we have the station level predictors for the intercept and trend (response) coefficients at the second level. We model the dependence among the climate trend coefficients using a multivariate normal distribution with the means informed by the station level predictors and a 4×4 covariance matrix Σ estimated using the observed data.

e. H_1 versus H_2

For any station, if the model proposed under H_2 is better (in terms of providing a reasonable summary of the data at hand) than the model proposed under H_1, we consider that the trends in the annual frequency of rainfall extremes can be better explained by the full suite of predictors as opposed to just GST. Further, we consider that the GST trend coefficient from the model proposed under H_2 is the real anthropogenic influence and the climate trend coefficients are the real climate controls. On the contrary, if the model proposed under H_2 is not an improvement over the model proposed under H_1, we hold that H_1 is the best alternate hypothesis that can explain the trends. We use posterior predictive checks (Rubin 1984) to evaluate and compare

the models for H_1 and H_2. The Akaike information criterion (AIC; Akaike 1998) and deviance information criterion (DIC; Spiegelhalter et al. 2002) are standard measures to check the prediction accuracy. Recently, Watanabe (2010) has proposed a fully Bayesian measure, the Watanabe–Akaike information criterion (WAIC), which closely approximates Bayesian cross-validation and is invariant to parameterization. Hence, we use the WAIC for estimating the pointwise prediction accuracy of the models. WAIC (also called the widely applicable information criterion) is seen as an improvement over DIC and can be estimated using the log-likelihood evaluated at the posterior simulations of the parameters (Vehtari et al. 2017).WAIC is computed as $-2\sum_{i=1}^{n}\log\int p(y_i\,|\,\theta)p_{\text{posterior}}(\theta)\,d\theta + 2p_{\text{waic}}$ (Vehtari et al. 2017), where the first term is the log pointwise predictive density and the second term is the estimated effective number of parameters calculated using the posterior variance of the log predictive density: $p_{\text{waic}} = \sum_{i=1}^{n}\text{var}_{\text{posterior}}[\log p(y_i\,|\,\theta)]$. Smaller values of the WAIC indicate better estimated predictive accuracy of the model. Readers are referred to Gelman et al. (1996) and Gelman et al. (2014) for an in-depth discussion on posterior predictive assessment of model fitness.

f. *Residual trend analysis*

For each station, we compute the residuals R_{it} of the best model chosen based on the WAIC criterion. The residuals from the models (H_1 or H_2) represent the values for Y_{it} after adjusting for exogenous variables, GST, and/or the four climate covariates (ENSO, NAO, PDO, and AMO). In other words, they reveal the variability in Y_{it} beyond what could be affiliated to the exogenous variables. Hence, the analysis of the time trends in R_{it} will help discern any unexplained trend after accounting for background variability. In the spirit of the Bayesian multilevel models, we fit the following model to the residuals:

$$R_{it} \sim N(\mu_{it}, \sigma_i^2), \tag{18}$$

$$\mu_{it} = \alpha_r^i + \beta_r^i t, \tag{19}$$

$$\alpha_r^i \sim N(a_{r0} + a_{r1}\overline{P}_i + a_{r2}\text{CV}_i + a_{r3}E_i, \sigma_{\alpha_r}^2), \quad \text{and} \tag{20}$$

$$\beta_r^i \sim N(b_{r0} + b_{r1}\overline{P}_i + b_{r2}\text{CV}_i + b_{r3}E_i, \sigma_{\beta_r}^2). \tag{21}$$

For each station i, we investigate whether the trend coefficient β_r^i is significantly different from zero or not. Similar to H_0, we compute the p value from the posterior distribution of β_r^i and evaluate its statistical significance at 1% level of significance. A p value less than the level of significance indicates that the residual trend coefficient β_r^i is statistically significant. Alternately, if the residual trend coefficient β_r^i is not significant, we infer that the trend initially observed in Y_{it} can be attributed to global temperature (if the residuals are obtained from H_1) or a combination of global temperature and cyclical climate (if the residuals are obtained from H_2).

g. *Choice of prior distributions, model fitting, and convergence*

For all the models, the joint posterior distribution $p(\boldsymbol{\theta}\,|\,\text{data})$ of the complete parameter vector is derived by combining the prior distributions and the likelihood functions. We assumed a uniform prior distribution for the variance terms and uninformative normal priors for the coefficients of the second level (Gelman 2006). The prior for the covariance matrix Σ is taken to be inverse Wishart distribution with an identity scale matrix $\mathbf{I}$ and 5 degrees of freedom (one more than the dimension of the matrix) (Gelman and Hill 2006).

The parameters are estimated using just another Gibbs sampler (JAGS; Plummer 2003; Denwood 2016), which employs the Gibbs sampler, a Markov chain Monte Carlo (MCMC) method for simulating the posterior probability distribution of the parameters conditional on the current choice of parameters and the data. Three consecutive chains are simulated using random initial values for the parameters. Each chain was run for 5000 cycles with 80% burn-in to discard the initial estimations. As Gelman and Rubin (1992) recommended, we monitor the convergence using a shrink factor. The ratio of variance between chains and variance within chains should be lower than 1.1.

5. Results and analysis

a. *Results from H_0*

In Fig. 3, we present the results from H_0, that there is no monotonic trend in the annual frequency of extreme rainfall events. The stations are shown as open circles where H_0 cannot be rejected and are filled with color where H_0 is rejected. We selected a 1% level to reject the null hypothesis. The color scheme indicates the direction (orange for increasing and blue for decreasing) and strength (expressed as percentage change from the mean per year) of the trend. While the stations in Colorado and Utah (Southwest climate region) show a negative trend, much of the country is dominated by a positive trend. We reject H_0 in 742 stations among the 1244 stations in our study. In Fig. 3 (bottom left), we show the percentage number of stations that exhibit a trend in each climate region. About 80% of the stations in the Upper Midwest and the Northeast climate regions exhibit an increasing trend. This is followed by the Ohio Valley and the South climate regions where 70% or more of the stations show an upward trend. Less than

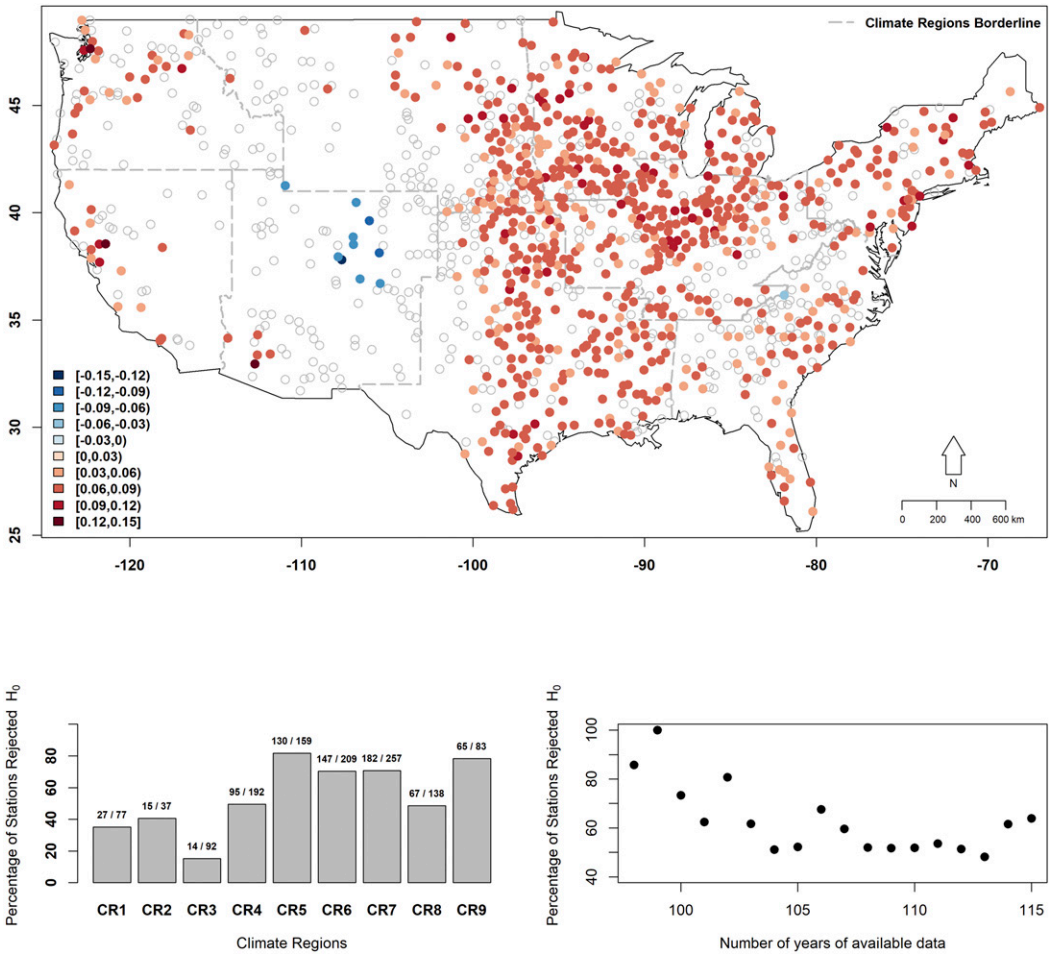

FIG. 3. (top) The spatial distribution of the stations that are significant at 99% confidence level—the values represent the median of posterior distribution of the time-trend coefficient. (bottom left) The bar charts for percentage of significant stations within each climate region. (bottom right) The dependency of the number of significant stations to the number of years of data.

50% of the stations in the other climate regions exhibit a trend. These results are consistent with previous findings from Groisman et al. (2004), Karl and Knight (1998), and Balling and Goodrich (2011). In Fig. 3 (bottom right), we show the percentage number of stations exhibiting trend as a function of sample size. For the 1244 stations, we identify how many stations exhibit significant trend under each category of sample size. For instance, among the seven stations with a sample size of 98 (number of years of complete data available), six stations exhibit a statistically significant trend (86%). From Fig. 3 (bottom right), we can see that the number of stations that show trends reduces substantially as the sample size (i.e., the number of years of available data increases). Having tested the null hypothesis and identified the locations that exhibit increasing or decreasing trends in the annual frequency of rainfall extremes, we next present our investigation on the possible factors to which the trend could be attributed: anthropogenic forcing or cyclical climate indicators or a combination thereof.

b. *Explaining the trends using H_1 and H_2*

In Fig. 4, we present the breakdown of the stations based on whether the trend is explained by any of the two hypotheses. The alternate hypothesis model choice is based on WAIC selection criterion. We performed a statistical significance test on the differences of WAIC for each stations based on a bootstrap resampling approach. Repeated draws from the posterior distribution are used to create a distribution of WAIC values for each model. These WAIC distributions are verified for significant differences using a KS test. Wherever the difference is statistically significant, we report the model with lower WAIC (H_1 or H_2) to have better predictive skill (i.e., a

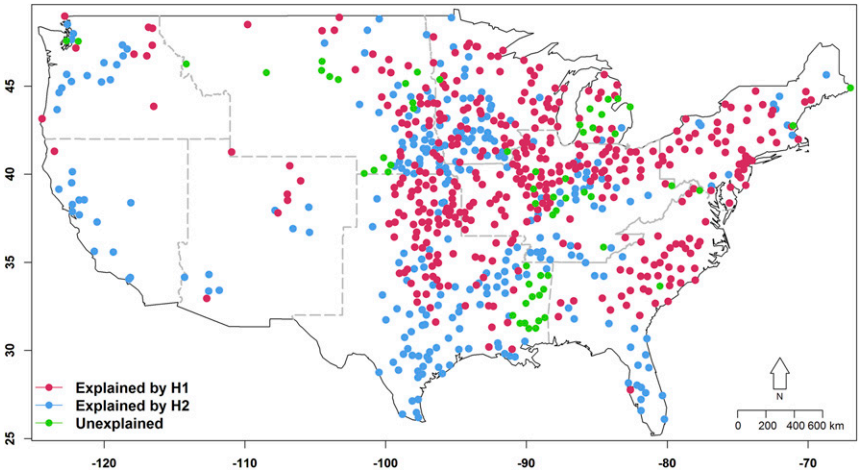

FIG. 4. The spatial distribution of stations explained by H_1 (where the monotonic trend in the annual frequency of extreme rainfall events is solely attributed to anthropogenic forcing) or H_2 (where monotonic trend in the annual frequency of extreme rainfall events is attributed to anthropogenic forcing and cyclical climate variability) or left unexplained.

better model that can represent the data). Among the 742 stations where H_0 (no monotonic time trend) is rejected, we identified 293 stations where the model proposed under H_2 offers better predictive accuracy ($\mathrm{WAIC}_{H_2} < \mathrm{WAIC}_{H_1}$) than the model proposed under H_1. In 274 of these stations (shown as blue dots in Fig. 4), there is no significant trend in the residuals (i.e., $\boldsymbol{\beta}_r$ values are indistinguishable from zero); hence, the trend initially observed can be explained by the combination of GST and climate signals with different quasi-periodicities. Most of the stations in the Northwest and West climate regions, and southern parts of South, Southeast, Upper Midwest, and Northern Rockies and Plains climate regions, fall under this category.

Similarly, among the 742 stations where H_0 is rejected, we identified 449 stations where the model proposed under H_1 offers better predictive accuracy ($\mathrm{WAIC}_{H_1} < \mathrm{WAIC}_{H_2}$) than the model proposed under H_2. In other words, adding climate information does not improve the model's predictive accuracy. In 409 of these stations (shown as red dots in Fig. 4), there is no significant trend in the residuals; hence, the trend initially observed can be affiliated to GST. Most of the stations in the Northeast, Ohio Valley, and Upper Midwest climate regions, and the northern parts of the South and Southeast climate regions, fall under this category. Generally, it is found that stations with high CV (rainfall year-to-year variability) responded to H_2 and stations with low CV responded to H_1.

c. *Attribution to climate change and climate variability modes*

Figure 5 provides the spatial distribution of the temperature response coefficient ($\boldsymbol{\beta}_1$ from H_1 in Fig. 5a and $\boldsymbol{\beta}_2$ from H_2 in Fig. 5b). A thick circle is shown for stations where $p(\beta > 0) > 0.9$ or $p(\beta > 0) < 0.1$. These are the stations that have strong positive or negative association with GST. The color scheme indicates the direction (orange for positive and blue for negative responses) and strength of association (i.e., the sensitivity expressed as percentage change from the mean per degree Celsius of global temperature). A conjunctive examination of Figs. 5a and 5b reveals that the stations in the Southeast climate region have $p(\beta > 0) < 0.9$, indicating a weaker association with GST. On the other hand, the stations in the Northeast, Ohio Valley, and Upper Midwest regions have a significant association with GST.

In Fig. 6, we present the spatial distribution of the response coefficients for the four climate covariates (ENSO, NAO, PDO, and AMO) for the stations represented by blue dots in Fig. 4 (i.e., where adding climate information improved the model predictive accuracy). The color scheme indicates the direction (orange for positive and blue for negative responses) and strength of association (i.e., the sensitivity expressed as percentage change from the mean per degree Celsius change in the climate indicator). Similar to Fig. 5, a thick circle is shown for stations where $p(\beta > 0) > 0.9$ or $p(\beta > 0) < 0.1$. These are the stations that have strong positive or negative association of rainfall extreme event frequency with the corresponding climate covariate. ENSO (Fig. 6a) has a significant positive relationship in southern Florida; the South, Ohio Valley, and Upper Midwest climate regions; and parts of California and Washington. These results are consistent with the results found in Gershunov and Cayan (2003), who have investigated the associations of ENSO

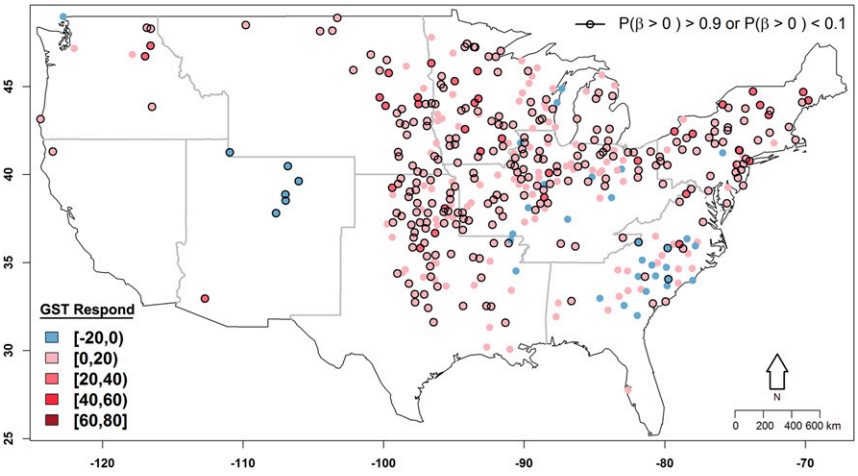

(a)

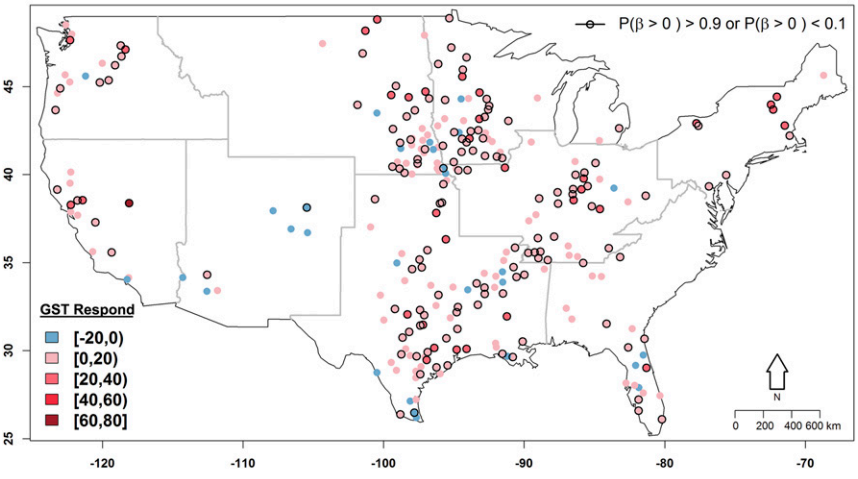

(b)

FIG. 5. The response to GST under (a) H_1 and (b) H_2. Thick circles are stations significant at the 90% confidence level.

with heavy precipitation events in the United States. The NAO (Fig. 6b) is found to have a positive (negative) connection with the stations in the Midwest (West) regions. PDO (Fig. 6c) replicates a pattern similar to ENSO, except in the South climate region where a north–south gradient is observed. The AMO (Fig. 6d) seems to have a significant negative association in much of the country, with dominance in stations in the Northern Rockies and Plains and Upper Midwest climate regions. In Fig. 6e, we present a summary of the climate influences (i.e., the number of stations responding to each climate predictor for each climate region). We consider a climate predictor to be significant if $p(\beta > 0) > 0.9$ or $p(\beta > 0) < 0.1$ from the posterior distribution of its trend coefficient. The South climate region is most significantly influenced by the climate covariates.

6. Summary and discussion

There has been much interest recently in identifying trends in hydrometeorological extreme events, and this has generated a rich body of literature that documented the magnitudes and spatial extents of the trends over the last century. While many of these works check for the hypothesis of no trend in the data using standard parametric/nonparametric tests, here we introduce a framework for trend detection and attribution process using a set of models (hypotheses) to compare. We start by asking the question of whether the underlying process of the data is invariant with time. Hence, we test the hypothesis that the series is a random draw from a probability distribution (Poisson distribution in our case) with the mean not changing over time. Since trends may be due to an

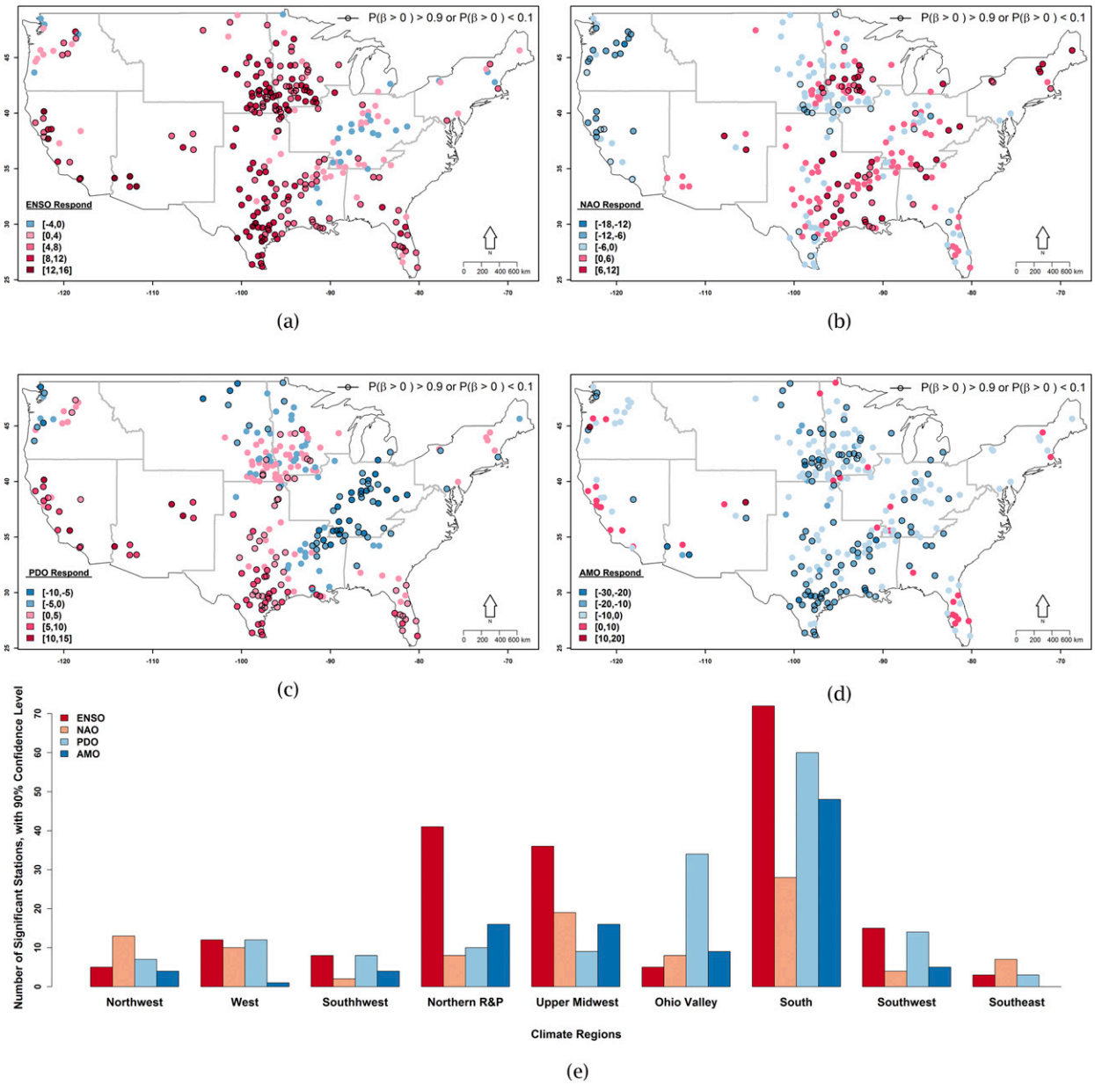

FIG. 6. The response to different climate variables, (a) ENSO, (b) NAO, (c) PDO, and (d) AMO, coming from H_2. Thick circles are stations significant at the 90% confidence level. (e) The breakdown of response to each climate variable over different climate regions.

influence of exogenous variables, we posit possible hypotheses (models) with these explanatory variables and recover the trend after their effect. A summary of this procedure is presented in Fig. 7.

1) Among the 1244 high-quality stations in the contiguous United States that were tested for monotonic trend in the frequency of extreme rainfall events using the Bayesian multilevel model, we find that in 502 stations the H_0 (where there is no trend) cannot be rejected, whereas in the remaining 742 stations it is rejected.
2) We postulated two hypotheses that the monotonic time trend observed in the frequency of rainfall extremes is (i) solely due to anthropogenic forcing [H_1 was tested using globally averaged near-surface temperature (GST) as an exogenous variable] and (ii) partly due to anthropogenic forcing and partly due to cyclical climate influences (H_2 was tested using GST and four climate covariates—ENSO, NAO, PDO and AMO—with varying quasiperiodicities). Among the 742 stations where H_0 is rejected, we find that in 449 stations, the model proposed

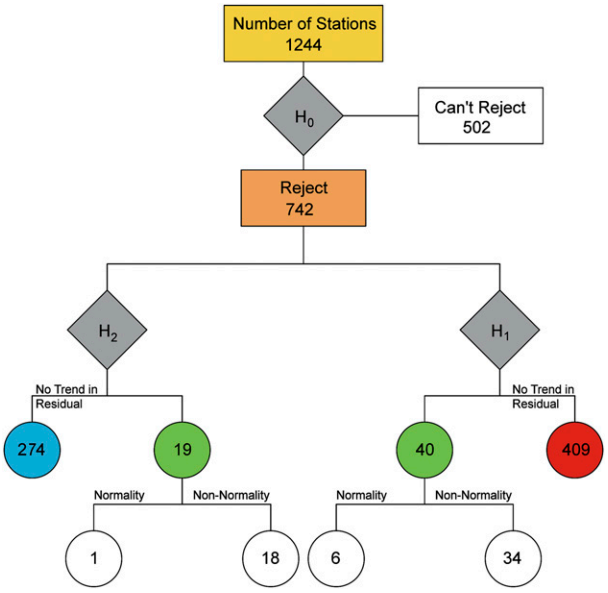

FIG. 7. A diagram summarizing the steps of study. Of the 1244 stations used for the study, 742 stations show time trends. Of these, 409 stations can be attributed to global temperature anomalies, and 274 stations can be attributed to global temperature and climate variables. The remaining 59 stations still show a time trend.

under H_1 offers better predictive ability. In the remaining 293 stations, inclusion of climate indices improved the predictability. This classification is based on a new fully Bayesian pointwise predictive accuracy criterion, the WAIC (Vehtari et al. (2017). We also tested a hypothesis with only climate predictors and found that the results are subset of the H_2 model. The stations that are best attributed to H_2 and do not exhibit a statistical significance for GST belong to this intermediate model.

3) Of the 449 stations where H_1 offers a reasonable summary of the data at hand, in 409 stations the residual trend is nonexistent, indicating that the trend initially observed in H_0 may be attributed to GST, or that H_1 best explains this trend. In 34 of the remaining 40 stations, we found that the residuals are not normally distributed. Six of them still exhibit a monotonic trend after accounting for GST.
4) Of the 293 stations where H_2 offers a reasonable summary of the data at hand, in 274 stations the residual trend is nonexistent. Hence, the trend initially observed in H_0 may be attributed to a combination of GST and the climate influences ENSO, NAO, PDO, and AMO. The H_2 best explains this trend. Of the remaining 19 stations, 18 have nonnormal residuals, indicating possible drivers other than the climate proxies applied in this study.
5) The spatial distribution of the corresponding influences of GST and the four climate covariates is provided in Figs. 5 and 6 along with the location of the stations where the influence is strong [$p(\beta > 0) > 0.9$ or $p(\beta > 0) < 0.1$].

Finally, a summary of this trend analysis and attribution for each climate region is provided in Table 1. In most of the stations in the Northwest, West, and Southwest climate regions, the observed monotonic time trend in the frequency of extreme rainfall events can be attributed to both climate change and climate variability modes (best explained by H_2). The Southeast and Northeast climate regions are dominated by stations (15.4% in the Southeast and 31.3% in the Northeast) where the trend can be attributed to GST. In the central and midwestern United States (Northern Rockies and Plains, Upper Midwest, Ohio Valley, and South regions) there is almost an even breakdown of the stations where the trend can be attributed solely to GST or to a combination of GST and climate.

We have approached this problem in an exploratory spirit and formulated possible hypotheses (based on known theoretical arguments) to support or falsify following the data analysis. We see that trends in the eastern half of the country can be largely attributed to changing temperatures, and at least the chosen climate variables have little influence. In the western half of the

TABLE 1. The number of stations explained by H_1 and H_2 or left unexplained, within each climate region (in the form No. of explained or unexplained stations in region divided by the total stations in region, followed by the percentage in parentheses).

Climate regions	Explained by H_1	Explained by H_2	Unexplained
Northwest	9/27 (33.3%)	16/27 (59.3%)	2/27 (7.4%)
West	1/15 (6.7%)	14/15 (93.3%)	0/15 (0%)
Southwest	6/14 (42.9%)	8/14 (57.1%)	0/14 (0%)
Northern Rockies and Plains	37/95 (38.9%)	43/95 (45.3%)	15/95 (15.8%)
Upper Midwest	77/130 (59.2%)	42/130 (32.3%)	11/130 (8.5%)
Ohio Valley	99/147 (67.3%)	36/147 (24.5%)	12/147 (8.2%)
South	83/182 (45.6%)	84/182 (46.2%)	15/182 (8.2%)
Southeast	44/67 (65.7%)	21/67 (31.3%)	2/67 (3%)
Northeast	53/65 (81.5%)	10/65 (15.4%)	2/65 (3.1%)

country, there is clearly a combined effect of changing temperature and large-scale cyclical climate variability. We conclude this work by providing the following caveats. The time series (both observed variables Y_{it} and exogenous variables) may have substantial autocorrelation structure that may manifest as apparent trends in limited data. Detection of autocorrelation before ascribing trends is important. While we did not explicitly test an autocorrelated model, we investigated for any autocorrelation in the residuals after accounting for the exogenous variables. In the 683 stations where the trend in the residuals is nonexistent, we also found that there is no autocorrelation in the residuals. A related caution here is that the exogenous variable could itself have a time series structure, which we did not consider in this paper. Further, we did not examine the effect of lagged dependence of the climate variables and their interactions here. One can develop models where an appropriate lag can be chosen based on model performance. One can also include climate variables' interaction based on the well-established theories. For example, in the western United States, there is a greater effect of climate modes when PDO and ENSO are in phase (Gershunov 1998; McCabe and Dettinger 1999). Such interactions can be included as part of the model framework. Furthermore, we have only demonstrated a generalized linear model here. Clearly, one can implement the methodology using nonparametric models and nonlinear trend detections. These are all part of our current investigation.

Acknowledgments. This research was supported by the NOAA-CREST Cooperative agreement NA11SEC4810004 and NSF Grant 1360446 (Water Sustainability and Climate, Category 3). The statements contained within the manuscript/research article are not the opinions of the funding agency or the U.S. government but reflect the authors' opinions.

REFERENCES

Akaike, H., 1998: Information theory and an extension of the maximum likelihood principle. *Selected Papers of Hirotugu Akaike*, E. Parzen, K. Tanabe, and G. Kitagawa, Eds., Springer, 199–213, https://doi.org/10.1007/978-1-4612-1694-0_15.

Alexander, L. V., and Coauthors, 2006: Global observed changes in daily climate extremes of temperature and precipitation. *J. Geophys. Res.*, **111**, D05109, https://doi.org/10.1029/2005JD006290.

Alfieri, L., P. Burek, L. Feyen, and G. Forzieri, 2015: Global warming increases the frequency of river floods in Europe. *Hydrol. Earth Syst. Sci.*, **19**, 2247–2260, https://doi.org/10.5194/hess-19-2247-2015.

Archambault, H. M., L. F. Bosart, D. Keyser, and A. R. Aiyyer, 2008: Influence of large-scale flow regimes on cool-season precipitation in the northeastern United States. *Mon. Wea. Rev.*, **136**, 2945–2963, https://doi.org/10.1175/2007MWR2308.1.

Asadieh, B., and N. Y. Krakauer, 2015: Global trends in extreme precipitation: Climate models versus observations. *Hydrol. Earth Syst. Sci.*, **19**, 877–891, https://doi.org/10.5194/hess-19-877-2015.

Balling, R. C., and G. B. Goodrich, 2011: Spatial analysis of variations in precipitation intensity in the USA. *Theor. Appl. Climatol.*, **104**, 415–421, https://doi.org/10.1007/s00704-010-0353-0.

Cai, W., and P. van Rensch, 2012: The 2011 southeast Queensland extreme summer rainfall: A confirmation of a negative Pacific decadal oscillation phase? *Geophys. Res. Lett.*, **39**, L08702, https://doi.org/10.1029/2011GL050820.

Castello, A. F., and M. L. Shelton, 2004: Winter precipitation on the US Pacific coast and El Niño–Southern Oscillation events. *Int. J. Climatol.*, **24**, 481–497, https://doi.org/10.1002/joc.1011.

Cayan, D. R., K. T. Redmond, and L. G. Riddle, 1999: ENSO and hydrologic extremes in the western United States. *J. Climate*, **12**, 2881–2893, https://doi.org/10.1175/1520-0442(1999)012<2881:EAHEIT>2.0.CO;2; Corrigendum, **12**, 3516, https://doi.org/10.1175/1520-0442(1999)012<3516:C>2.0.CO;2.

Cioffi, F., U. Lall, E. Rus, and C. K. B. Krishnamurthy, 2015: Space-time structure of extreme precipitation in Europe over the last century. *Int. J. Climatol.*, **35**, 1749–1760, https://doi.org/10.1002/joc.4116.

Coles, S. G., and J. A. Tawn, 1996: Modelling extremes of the areal rainfall process. *J. Roy. Stat. Soc.*, **58B**, 329–347.

Cooley, D., D. Nychka, and P. Naveau, 2007: Bayesian spatial modeling of extreme precipitation return levels. *J. Amer. Stat. Assoc.*, **102**, 824–840, https://doi.org/10.1198/016214506000000780.

Curtis, S., 2008: The Atlantic multidecadal oscillation and extreme daily precipitation over the US and Mexico during the hurricane season. *Climate Dyn.*, **30**, 343–351, https://doi.org/10.1007/s00382-007-0295-0.

Denwood, M. J., 2016: runjags: An R package providing interface utilities, model templates, parallel computing methods and additional distributions for MCMC models in JAGS. *J. Stat. Software*, **71**, 1–25, https://doi.org/10.18637/jss.v071.i09.

Durkee, J. D., J. D. Frye, C. M. Fuhrmann, M. C. Lacke, H. G. Jeong, and T. L. Mote, 2008: Effects of the North Atlantic Oscillation on precipitation-type frequency and distribution in the eastern United States. *Theor. Appl. Climatol.*, **94**, 51–65, https://doi.org/10.1007/s00704-007-0345-x.

Eichler, T., and W. Higgins, 2006: Climatology and ENSO-related variability of North American extratropical cyclone activity. *J. Climate*, **19**, 2076–2093, https://doi.org/10.1175/JCLI3725.1.

Enfield, D. B., A. M. Mestas-Nuñez, and P. J. Trimble, 2001: The Atlantic multidecadal oscillation and its relationship to rainfall and river flows in the continental U.S. *Geophys. Res. Lett.*, **28**, 2077–2080, https://doi.org/10.1029/2000GL012745.

Fischer, E. M., and R. Knutti, 2014: Detection of spatially aggregated changes in temperature and precipitation extremes. *Geophys. Res. Lett.*, **41**, 547–554, https://doi.org/10.1002/2013GL058499.

Gelman, A., 2006: Prior distributions for variance parameters in hierarchical models (comment on article by Browne and Draper). *Bayesian Anal.*, **1**, 515–534, https://doi.org/10.1214/06-BA117A.

——, and D. B. Rubin, 1992: Inference from iterative simulation using multiple sequences. *Stat. Sci.*, **7**, 457–472, https://doi.org/10.1214/ss/1177011136.

——, and J. Hill, 2006: *Data Analysis Using Regression and Multilevel/Hierarchical Models*. 1st ed. Cambridge University Press, 625 pp.

——, X. L. Meng, and H. Stern, 1996: Posterior predictive assessment of model fitness via realized discrepancies. *Stat. Sin.*, **6**, 733–760.

——, J. B. Carlin, H. S. Stern, and D. B. Rubin, 2003: *Bayesian Data Analysis*. 2nd ed. Texts in Statistical Science Series, Vol. 60, Chapman & Hall/CRC, 667 pp.

——, J. Hwang, and A. Vehtari, 2014: Understanding predictive information criteria for Bayesian models. *Stat. Comput.*, **24**, 997–1016, https://doi.org/10.1007/s11222-013-9416-2.

Gergis, J., and B. J. Henley, 2017: Southern Hemisphere rainfall variability over the past 200 years. *Climate Dyn.*, **48**, 2087–2105, https://doi.org/10.1007/s00382-016-3191-7.

Gershunov, A., 1998: ENSO influence on intraseasonal extreme rainfall and temperature frequencies in the contiguous United States: Implications for long-range predictability. *J. Climate*, **11**, 3192–3203, https://doi.org/10.1175/1520-0442(1998)011<3192:EIOIER>2.0.CO;2.

——, and D. R. Cayan, 2003: Heavy daily precipitation frequency over the contiguous United States: Sources of climatic variability and seasonal predictability. *J. Climate*, **16**, 2752–2765, https://doi.org/10.1175/1520-0442(2003)016<2752:HDPFOT>2.0.CO;2.

Goodrich, G. B., 2007: Influence of the Pacific decadal oscillation on winter precipitation and drought during years of neutral ENSO in the western United States. *Wea. Forecasting*, **22**, 116–124, https://doi.org/10.1175/WAF983.1.

Groisman, P. Ya., R. W. Knight, T. R. Karl, D. R. Easterling, B. Sun, and J. H. Lawrimore, 2004: Contemporary changes of the hydrological cycle over the contiguous United States: Trends derived from in situ observations. *J. Hydrometeor.*, **5**, 64–85, https://doi.org/10.1175/1525-7541(2004)005<0064:CCOTHC>2.0.CO;2.

Hansen, J., R. Ruedy, M. Sato, and K. Lo, 2010: Global surface temperature change. *Rev. Geophys.*, **48**, RG4004, https://doi.org/10.1029/2010RG000345.

Haylock, M. R., and Coauthors, 2006: Trends in total and extreme South American rainfall in 1960–2000 and links with sea surface temperature. *J. Climate*, **19**, 1490–1512, https://doi.org/10.1175/JCLI3695.1.

Hennessy, K. J., J. M. Gregory, and J. F. B. Mitchell, 1997: Changes in daily precipitation under enhanced greenhouse conditions. *Climate Dyn.*, **13**, 667–680, https://doi.org/10.1007/s003820050189.

Huntington, T. G., 2006: Evidence for intensification of the global water cycle: Review and synthesis. *J. Hydrol.*, **319**, 83–95, https://doi.org/10.1016/j.jhydrol.2005.07.003.

IPCC, 2013: Summary for policymakers. *Climate Change 2013: The Physical Science Basis*, T. F. Stocker et al., Eds., Cambridge University Press, 3–29.

Kamruzzaman, M., S. Beecham, and A. V. Metcalfe, 2013: Climatic influences on rainfall and runoff variability in the southeast region of the Murray-Darling basin. *Int. J. Climatol.*, **33**, 291–311, https://doi.org/10.1002/joc.3422.

Karl, T. R., and W. J. Koss, 1984: Regional and national monthly, seasonal, and annual temperature weighted by area, 1895–1983. National Climatic Data Center Tech. Rep. Historical Climatology Series 4-3, 38 pp.

——, and R. W. Knight, 1998: Secular trends of precipitation amount, frequency, and intensity in the United States. *Bull. Amer. Meteor. Soc.*, **79**, 231–241, https://doi.org/10.1175/1520-0477(1998)079<0231:STOPAF>2.0.CO;2.

Mantua, N. J., and S. R. Hare, 2002: The Pacific decadal oscillation. *J. Oceanogr.*, **58**, 35–44, https://doi.org/10.1023/A:1015820616384.

McCabe, G. J., and M. D. Dettinger, 1999: Decadal variations in the strength of ENSO teleconnections with precipitation in the western United States. *Int. J. Climatol*, **19**, 1399–1410, https://doi.org/10.1002/(SICI)1097-0088(19991115)19:13<1399::AID-JOC457>3.0.CO;2-A.

Meehl, G. A., C. Tebaldi, H. Teng, and T. C. Peterson, 2007: Current and future U.S. weather extremes and El Niño. *Geophys. Res. Lett.*, **34**, L20704, https://doi.org/10.1029/2007GL031027.

Min, S.-K., X. Zhang, F. W. Zwiers, and G. C. Hegerl, 2011: Human contribution to more-intense precipitation extremes. *Nature*, **470**, 378–381, https://doi.org/10.1038/nature09763.

Parr, D., G. Wang, and K. F. Ahmed, 2015: Hydrological changes in the U.S. Northeast using the Connecticut River basin as a case study: Part 2. Projections of the future. *Global Planet. Change*, **133**, 167–175, https://doi.org/10.1016/j.gloplacha.2015.08.011.

Plummer, M., 2003: JAGS: A program for analysis of Bayesian graphical models using Gibbs sampling. *Proc. Third Int. Workshop on Distributed Statistical Computing (DSC 2003)*, Vienna, Austria, R Foundation for Statistical Computing, https://www.r-project.org/conferences/DSC-2003/Proceedings/Plummer.pdf.

Renard, B., 2011: A Bayesian hierarchical approach to regional frequency analysis. *Water Resour. Res.*, **47**, W11513, https://doi.org/10.1029/2010WR010089.

——, X. Sun, and M. Lang, 2013: Bayesian methods for non-stationary extreme value analysis. *Extremes in a Changing Climate*, A. AghaKouchak et al., Eds., Water Science and Technology Library, Vol. 65, Springer, 39–95, https://doi.org/10.1007/978-94-007-4479-0_3.

Ring, M. J., D. Lindner, E. F. Cross, and M. E. Schlesinger, 2012: Causes of the global warming observed since the 19th century. *Atmos. Climate Sci.*, **2**, 401–415, https://doi.org/10.4236/acs.2012.24035.

Rubin, D. B., 1984: Bayesianly justifiable and relevant frequency calculations for the applied statistician. *Ann. Stat.*, **12**, 1151–1172, https://doi.org/10.1214/aos/1176346785.

Samuel, J. M., and M. Sivapalan, 2008: A comparative modeling analysis of multiscale temporal variability of rainfall in Australia. *Water Resour. Res.*, **44**, W07401, https://doi.org/10.1029/2007WR006373.

Sang, H., and A. E. Gelfand, 2010: Continuous spatial process models for spatial extreme values. *J. Agric. Biol. Environ. Stat.*, **15**, 49–65, https://doi.org/10.1007/s13253-009-0010-1.

Schliep, E. M., D. Cooley, S. R. Sain, and J. A. Hoeting, 2010: A comparison study of extreme precipitation from six different regional climate models via spatial hierarchical modeling. *Extremes*, **13**, 219–239, https://doi.org/10.1007/s10687-009-0098-2.

Schreck, C. J., III, and F. H. M. Semazzi, 2004: Variability of the recent climate of eastern Africa. *Int. J. Climatol.*, **24**, 681–701, https://doi.org/10.1002/joc.1019.

Scian, B., and J. Pierini, 2013: Variability and trends of extreme dry and wet seasonal precipitation in Argentina. A retrospective analysis. *Atmósfera*, **26**, 3–26, https://doi.org/10.1016/S0187-6236(13)71059-2.

Seneviratne, S. I., and Coauthors, 2012: Changes in climate extremes and their impacts on the natural physical environment. *Managing the Risks of Extreme Events and Disasters to Advance Climate Change Adaptation*, C. B. Field et al., Eds., Cambridge University Press, 109–230, https://www.ipcc.ch/pdf/special-reports/srex/SREX-Chap3_FINAL.pdf.

Spiegelhalter, D. J., N. G. Best, B. P. Carlin, and A. Van Der Linde, 2002: Bayesian measures of model complexity and fit. *J. Roy. Stat. Soc.*, **64B**, 583–639, https://doi.org/10.1111/1467-9868.00353.

Sun, X., and U. Lall, 2015: Spatially coherent trends of annual maximum daily precipitation in the United States. *Geophys. Res. Lett.*, **42**, 9781–9789, https://doi.org/10.1002/2015GL066483.

——, M. Thyer, B. Renard, and M. Lang, 2014: A general regional frequency analysis framework for quantifying local-scale climate effects: A case study of ENSO effects on southeast Queensland rainfall. *J. Hydrol.*, **512**, 53–68, https://doi.org/10.1016/j.jhydrol.2014.02.025.

Sutton, R., E. Suckling, and E. Hawkins, 2015: What does global mean temperature tell us about local climate? *Philos. Trans. Roy. Soc.*, **373A**, 20140426, https://doi.org/10.1098/rsta.2014.0426.

Teegavarapu, R. S. V., A. Goly, and J. Obeysekera, 2013: Influences of Atlantic multidecadal oscillation phases on spatial and temporal variability of regional precipitation extremes. *J. Hydrol.*, **495**, 74–93, https://doi.org/10.1016/j.jhydrol.2013.05.003.

Trenberth, K. E., 2011: Changes in precipitation with climate change. *Climate Res.*, **47**, 123–138, https://doi.org/10.3354/cr00953.

——, A. Dai, R. M. Rasmussen, and D. B. Parsons, 2003: The changing character of precipitation. *Bull. Amer. Meteor. Soc.*, **84**, 1205–1217, https://doi.org/10.1175/BAMS-84-9-1205.

van Oldenborgh, G. J., L. A. te Raa, H. A. Dijkstra, and S. Y. Philip, 2009: Frequency- or amplitude-dependent effects of the Atlantic meridional overturning on the tropical Pacific Ocean. *Ocean Sci.*, **5**, 293–301, https://doi.org/10.5194/os-5-293-2009.

Vehtari, A., A. Gelman, and J. Gabry, 2017: Practical Bayesian model evaluation using leave-one-out cross-validation and WAIC. *Stat. Comput.*, **27**, 1413–1432, https://doi.org/10.1007/s11222-016-9696-4.

Verdon, D. C., A. M. Wyatt, A. S. Kiem, and S. W. Franks, 2004: Multidecadal variability of rainfall and streamflow: Eastern Australia. *Water Resour. Res.*, **40**, W10201, https://doi.org/10.1029/2004WR003234.

Villarini, G., J. A. Smith, M. L. Baeck, R. Vitolo, D. B. Stephenson, and W. F. Krajewski, 2011: On the frequency of heavy rainfall for the Midwest of the United States. *J. Hydrol.*, **400**, 103–120, https://doi.org/10.1016/j.jhydrol.2011.01.027.

Watanabe, S., 2010: Asymptotic equivalence of Bayes cross validation and widely applicable information criterion in singular learning theory. *J. Mach. Learn. Res.*, **11**, 3571–3594.

Westra, S., L. V. Alexander, and F. W. Zwiers, 2013: Global increasing trends in annual maximum daily precipitation. *J. Climate*, **26**, 3904–3918, https://doi.org/10.1175/JCLI-D-12-00502.1.

——, B. Renard, and M. Thyer, 2015: The ENSO–precipitation teleconnection and its modulation by the interdecadal Pacific oscillation. *J. Climate*, **28**, 4753–4773, https://doi.org/10.1175/JCLI-D-14-00722.1.

Willems, P., 2013: Adjustment of extreme rainfall statistics accounting for multidecadal climate oscillations. *J. Hydrol.*, **490**, 126–133, https://doi.org/10.1016/j.jhydrol.2013.03.034.

Zhang, R., and T. L. Delworth, 2006: Impact of Atlantic multidecadal oscillations on India/Sahel rainfall and Atlantic hurricanes. *Geophys. Res. Lett.*, **33**, L17712, https://doi.org/10.1029/2006GL026267.

Zhu, J., 2013: Impact of climate change on extreme rainfall across the United States. *J. Hydrol. Eng.*, **18**, 1301–1309, https://doi.org/10.1061/(ASCE)HE.1943-5584.0000725.